In-Situ Transmission Electron Microscopy Study of the Nanoindentation Behavior of Al

A.M. MINOR,[1,2,4] E.T. LILLEODDEN,[2] E.A. STACH,[3] and J.W. MORRIS, Jr.[1,2]

1.—Department of Materials Science and Engineering, University of California, Berkeley, CA 94720. 2.—Materials Science Division, Lawrence Berkeley National Laboratory, Berkeley, CA 94720. 3.—National Center for Electron Microscopy, Lawrence Berkeley National Laboratory. 4.—E-mail: aminor@lbl.gov

Nanoindentation is a useful technique for investigating fundamental mechanisms associated with small-volume deformation, processes that are often obscured on coarser scales. Recently, a novel experimental technique of in-situ nanoindentation for the transmission electron microscope (TEM), which provides real-time observations of the mechanisms associated with localized deformation, has been developed. Calibration of the force-displacement-voltage relation and load-frame compliance associated with this instrument allows quantitative force-displacement measurements to be obtained in the manner of traditional indentation experiments. Here, we describe the experimental technique along with methods for quantifying the load-displacement response. Additionally, results from experiments into Al thin films are presented.

Key words: Nanoindentation, in-situ TEM, Al, thin films, grain size

INTRODUCTION

The emergence of nanotechnology has heightened the importance of understanding the mechanical properties of nanoscale volumes of solids. The technique of nanoindentation has been developed as a method to probe the mechanical properties of materials in the submicron size range,[1,2] which is a typical dimension of the thin films used in integrated circuits and microelectromechanical systems. In typical nanoindentation experiments, the sample surface is indented with a sharp diamond pyramid, which has a tip that can be characterized by a radius of curvature on the order of 100 nm. Both elastic and plastic deformation results in the sample. The displacements imposed during nanoindentation are on the order of nanometers, and high-resolution load and displacement measurements are simultaneously recorded. Thus, it is possible to study atomistic-scale deformation process, such as dislocation nucleation events[3,4] and pressure-induced phase transformations.[5]

A multitude of behaviors have been observed with "instrumented" indentation techniques,[6] although important direct observations of the associated mechanisms of deformation are lacking. Because of the small volume of deformation associated with

nanoindentation experiments, the fundamental processes associated with the initiation of plasticity in initially dislocation-free material can be studied with this technique. A common observation made in nanoindentation experiments is a discrete displacement burst, or so-called "pop-in," corresponding to the deviation from Hertzian elastic behavior.[3,4,7] This pop-in response is typically associated with the nucleation of dislocations. Hertzian elastic theory[8] predicts that the nucleation event occurs below the surface along the axis of the indenter. However, the idealizations made in these models may not be appropriate. The real conditions of contact friction as well as the presence of thin surface layers (e.g., native oxides) may affect the position and character of the nucleation event. That is to say that nucleation from the native-oxide/metal interface may be a relevant mechanism, and it is unclear whether prismatic-loop nucleation or shear-loop nucleation is occurring. To resolve these issues, direct observation of evidence of the deformation mechanisms is needed and is obtainable only in situ.

EXPERIMENTAL TECHNIQUE

A sample holder for in-situ nanoindentation in an electron microscope was developed previously.[9,10] A diamond indenter is rigidly attached to a piezoceramic crystal, which will displace when a voltage is

applied. The diamond indenter is doped with boron to make it electrically conductive in the microscope. The indentation is made perpendicular to the direction of the electron beam, allowing real-time imaging of the imposed deformation. Unique sample geometries are needed to make the sample transparent to electrons. Here, we have used lithographically prepared, Si substrates onto which a thin film of the material of interest is deposited. The Si substrates are first etched to produce wedgelike structures. The top of the wedge is a small plateau approximately 150-nm wide. An Al film is evaporated at 300°C across the entire Si structure, and an indentation is made into the cap of the film on top of the plateau. The grain size varies between approximately 50–700 nm and is topographically smooth except for the expected cusps at the grain boundaries. A scanning electron micrograph of this test structure is given in Fig. 1, which shows a cross-sectional view of a 250-nm-thick Al film on the Si wedge along with the indentation and electron-beam directions. The nominal grain size is one to two times the film thickness, while the nominal radius of curvature of the indenter tip is 50–75 nm. Thus, grain centers can be indented such that the deforming body can be approximated as a single crystal.

In contrast to conventional indentation techniques, which provide high-resolution load and displacement measurements, the load applied to the sample during in-situ indentation is not measured directly. This is because indentation of the tip into the sample is controlled through the voltage applied to the piezoceramic element, which leads to a load that is dependent on both the voltage applied to the piezoceramic crystal and the resulting displacement during indentation. The voltage is the imposed (independent) variable, while the displacement is measured directly from the real-time imaging of the indentation process.

The relationship between the voltage applied to the piezoceramic element, the displacement of the indenter, and the force applied to the sample can be derived using a simple spring-dashpot model of the indentation system. This model is shown schematically in Fig. 2. The stiffness of the piezoceramic crystal is represented by k_{PZ}, the stiffness of the indenter is described by $k_{indenter}$, and the stiffness of the gripping system, which is dominated by a Teflon (DuPont Corp., Wilmington, DE) ring, is given by k_{teflon}. The piezoelectric coefficient is described by d_{PZ}, and k_s is the contact stiffness. To calibrate our load frame for the constants described earlier and, hence, establish a general relationship for the load-displacement behavior during indentation, a series of experiments were conducted on Si cantilevers where the bending stiffnesses were known. The derivation of the general relationship for quantitative voltage-controlled mechanical testing will now be described.

Let us first consider the displacement of the indenter assembly with an applied voltage, V, under the condition of no constraint (e.g., no sample contact), as shown in Fig. 2a. This is equivalent to zero applied force, and the displacement is proportional to the applied voltage:

$$\Delta x_{PZ}^0 = d_{PZ}\, V \qquad (1)$$
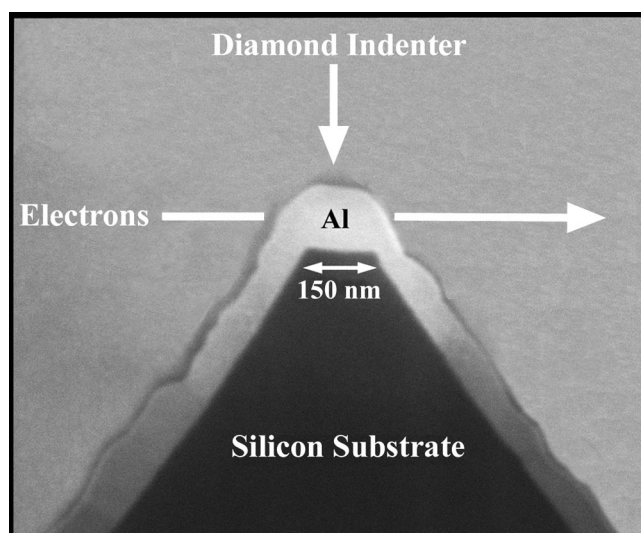
Next, when the indenter is in contact with the

Fig. 1. The SEM cross-sectional image of the in-situ, nanoindentation sample configuration and its orientation relative to the electron beam and indentation direction. A 250-nm Al film deposited onto a Si wedge structure is shown. The film thickness appears <250 nm because of the 52° tilt of the sample.
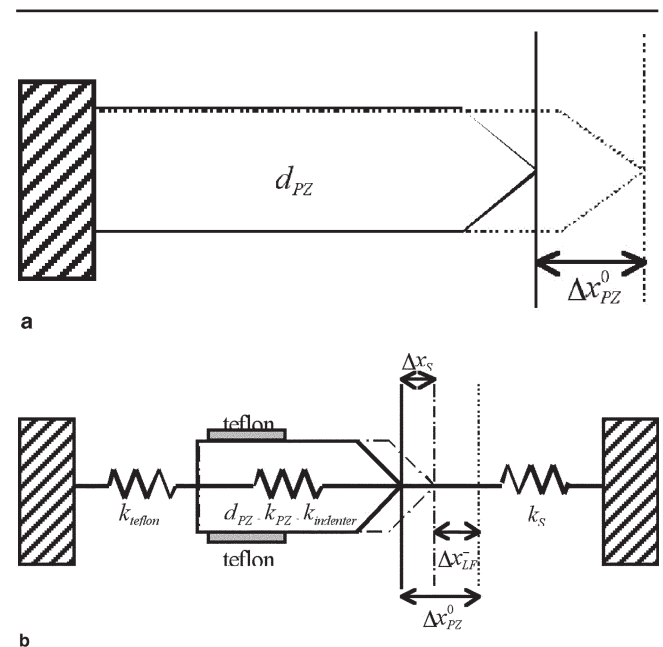

Fig. 2. (a) The schematic of the displacement of the indenter assembly with no sample contact. The solid line indicates the initial position of the assembly: $V^{app} = 0$, and $F^{app} = 0$. The dotted line shows the position of the assembly under the application of voltage: $V^{app} = V$, and $F^{app} = 0$. (b) Schematic description of the assembly in contact with a sample, where the various components act similar to springs in series. Again, the solid line is the initial position of the indenter/sample interface, and the dotted line shows the position of the indenter assembly under the application of a voltage if no sample was present. The dash-dot line shows the position of the indenter/sample interface under an applied voltage and sample constraint: $V^{app} = V$, and $F^{app} = F$.

sample (Fig. 2b), the indenter assembly no longer acts as a rigid solid that applies no force. Rather, a force, F, is applied to the sample, and the loading assembly can be described as a set of springs, as shown schematically in Fig. 2b. Because the rear of the indenter assembly, the piezoceramic crystal, and the Teflon grip are in series, the effective spring constant associated with the load-frame is given by

$$k_{LF} = \left\{ \frac{1}{k_{teflon}} + \frac{1}{k_{PZ}} + \frac{1}{k_{indenter}} \right\}^{-1} \quad (2)$$

In the loaded configuration, the total displacement of the indenter assembly is less than the unconstrained displacement, Δx_{PZ}^0, because of the resistance of the sample to the applied force and is given by

$$\Delta x_{PZ} = \Delta x_{PZ}^0 - \Delta x_{LF}^- \quad (3)$$

where Δx_{LF}^- is the backward displacement of the load frame, related to the force on the load-frame, F_{LF}, and the load-frame stiffness,

$$\Delta x_{LF}^- = \frac{F_{LF}}{k_{LF}} \quad (4)$$

The total displacement of the indenter tip is necessarily equal to the displacement of the sample, x_s, which is, in turn, equal to the sum of the bending displacement, $x_{Si,bend}$, and indentation displacements of the sample, $x_{Si,ind}$:

$$\Delta x_{PZ} = \Delta x_{Si,bend} + \Delta x_{Si,ind} \quad (5)$$

Assuming that the stiffness of the contact is much greater than the stiffness of the cantilever,* this simplifies to

$$\Delta x_{PZ} \approx \Delta x_{Si,bend} = \Delta x_{Si} \quad (6)$$

For a rectangular cross-section cantilever of constant width and thickness, the force applied to the cantilever, F_{Si}, is related to the bending displacement by

$$F_{Si} = k_{Si} \Delta x_{Si} \quad (7)$$

The bending stiffness of the cantilever, k_{Si}, is defined as

$$k_{Si} = E \frac{t^3 w}{4l^3} \quad (8)$$

where E is the Young's modulus of Si in the bending direction, and t, w, and l are the thickness, width, and lever-arm length of the cantilever, respectively. Invoking the condition of equilibrium, the force applied to the cantilever must be equal to the force applied to the load frame:

$$F_{LF} = F_{Si} = F \quad (9)$$

It is of interest to find a single relation between the force, displacement, and voltage in terms of the

---

*Or, if the voltage-displacement data is taken from the unloading portion of the experiment, there is no indentation at all. This was the case in our calibration experiments performed on silicon cantilevers.

known constant, k_{Si}, and the measured variables, V and Δx_{Si}. By combining Eqs. 3 and 6, we find

$$\Delta x_{Si} = \Delta x_{PZ}^0 - \Delta x_{LF}^- \quad (10a)$$

Substituting in Eqs. 1 and 4 leads to

$$\Delta x_{Si} = d_{PZ} V - \frac{F_{LF}}{k_{LF}} \quad (10b)$$

Then, using Eqs. 7 and 9, we find

$$\Delta x_{Si} = d_{PZ} V - \frac{k_{Si} \Delta x_{Si}}{k_{LF}} \quad (10c)$$

Rearranging terms, we find

$$\Delta x_{Si} = \frac{k_{LF}}{k_{Si} + k_{LF}} d_{PZ} V \quad (11)$$

which relates the measurable bending displacement of the Si cantilever to the applied voltage, the known stiffness of the cantilever, the unknown load-frame stiffness, and the unknown piezoelectric coefficient.

Two separate experiments can be conducted on a single Si cantilever to determine the two unknowns, k_{LF} and d_{PZ}. By concentrating the applied force at different positions along the length of the cantilever lever arm, one achieves different values of the bending stiffness, k_{Si}. Using results from two such experiments, the constants were determined to be $k_{LF} = 320$ N/m and $d_{PZ} = 1.96$ µm/V. Thus, the load-displacement-voltage relation describing an indentation experiment is given by inserting these constants into the following equation:

$$F_{sample} = k_{LF} (d_{PZ}V - \Delta x_{sample}) \quad (12)$$

Figure 3 shows an in-situ transmission electron microscope (TEM) image of the experiment in which the indenter bends a Si cantilever typically used for atomic force microscopy (AFM). The AFM imaging probe can be seen in the figure but does not affect the experimental results. The displacement of the

20 µm

silicon cantilever

diamond indenter

11:38:33 AM   si cant 5.3 mag 0.4kx
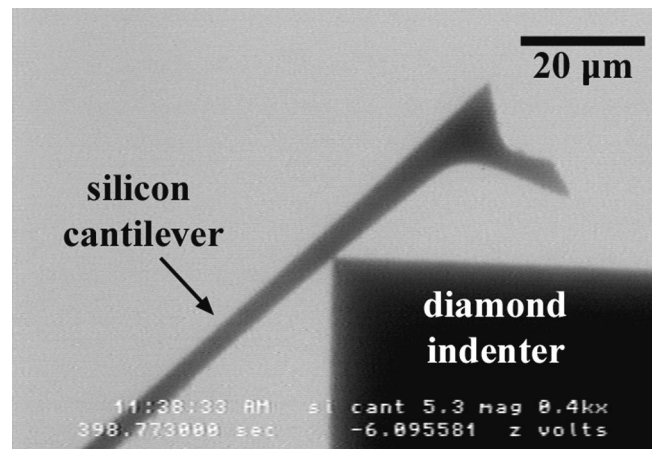398.773000 sec   -6.095581 z volts

Fig. 3. The TEM image of the diamond indenter in contact with a single-crystal silicon cantilever. The calibration constants for the load frame were determined from the unloading data of the silicon cantilever with the diamond positioned at two different places along the cantilever lever arm.

cantilever is directly measured from real-time images, as shown in Fig. 4, and is correlated to the voltage applied to the piezoceramic element along with the applied force, which is calculated from the known bending stiffness. Therefore, the force applied to the sample can be determined from the voltage applied to the piezoceramic element and the displacement measured in situ. This relationship is expressed through Eq. 12, and is shown schematically in Fig. 5.

RESULTS AND DISCUSSION

Thus far, all of our in-situ nanoindentation experiments have been performed on Al films deposited onto Si. Because the Peierl's barrier in Al is extremely low, and consequently, the dislocation velocity is fast, our video sampling rate of 30 frames per second is too slow to capture the movement of the individual dislocations. Hence, each video image captured during the in-situ experiments presented here is essentially a quasistatic image of the equilibrium configuration of defects. Figure 6 illustrates this point by showing a series of six images taken from a video during an in-situ nanoindentation experiment. In Fig. 6a, the diamond is approaching an Al grain that is approximately 400 nm in diameter. Figure 6b and c shows images of the evolution of the induced-stress contours during the initial stage of indentation and correspond to purely elastic deformation in the absence of any pre-existing dislocations that could cause plasticity. Figure 6d shows the first indication of plastic deformation, in which dislocations are nucleated; a set of prismatic loops is observed. Previous in-situ nanoindentation studies on similar samples have also shown the nucleation of prismatic loops.[10] Figure 6c and d are consecutive frames of the video and are 1/30 of a second apart. As can be seen, the exact location of the nucleation event is not discernable because the evolution of the dislocation configuration has already proceeded beyond the point at which that
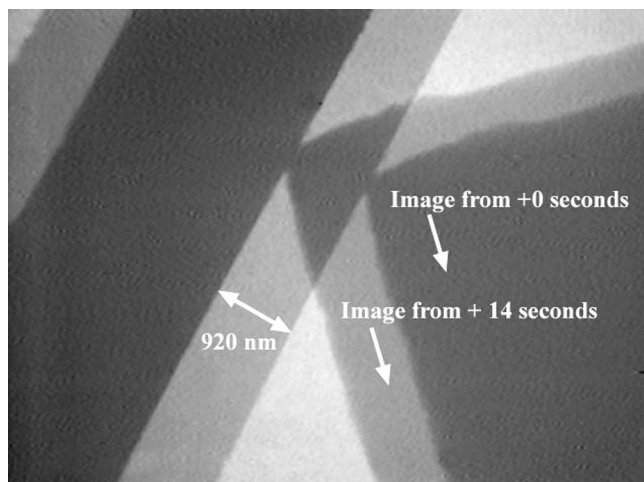

Fig. 4. The superimposed, in-situ TEM images of the calibration experiment on the Si cantilever shows the displacement of the beam relative to the reference position. The two superimposed images correspond to $\Delta x_{Si} = 0$, and $\Delta x_{Si} = 920$ nm.
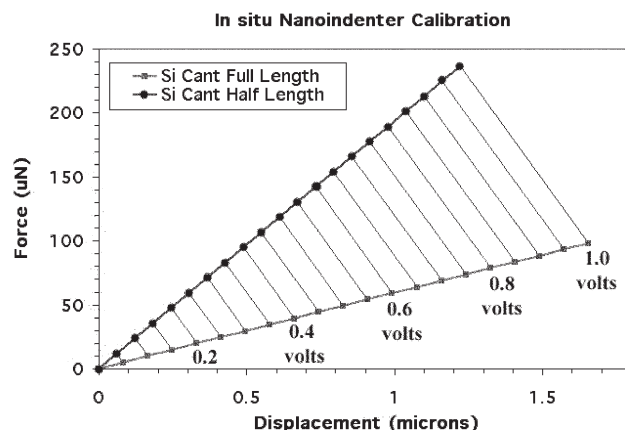

Fig. 5. The results from the Si-cantilever calibration experiments showing the basic relationship that, for a given voltage, the force and displacement behavior of an indentation are coupled.

might be possible. Figure 6e and f shows the large increase in dislocation density achieved as deformation proceeds and dislocations tangle and multiply.

Although the precise nucleation site may be difficult, if not impossible, to establish from such experiments, in-situ indentation experiments provide unique advantages over ex-situ TEM analysis of postindent dislocation configurations. In addition to the difficulty in preparing TEM samples after indentations have been conducted, the strong image forces exerted on the dislocations by the free surface can lead to very different structures after the sample has been unloaded. Indeed, in our studies, it has been observed that the configuration of defects changes dramatically after the dislocations have had time to rearrange themselves and, possibly, anneal out of the sample. During the in-situ experiments on the Al thin films, it is observed that the configuration of dislocations that result during loading is usually lost within minutes of unloading the sample. This observation suggests that postmortem TEM studies of indentation-induced plasticity should be viewed with some caution.

A previous study by Lilleodden and Nix showed that the indentation behavior of thin gold films showed characteristic differences in the loading behavior that was related to the grain size of the samples.[11,12] For a 1-μm-thick Au film, with an average grain size of 3 μm, it was found that the load-displacement response is similar to that found in bulk single crystals. The load-displacement behavior of this coarse-grained sample is presented in Fig. 7, showing Hertzian elastic response followed by discrete bursts of plasticity. This behavior has been termed "staircase" yielding[13] and is often observed in single crystalline samples. Figure 7 also shows the load-displacement behavior associated with indentation into a 160-nm Au film characterized by an average grain size of 100 nm. In contrast, the finer-grained sample resulted in continuous elastic-plastic loading from the onset of contact. A likely reason for this behavior is that dislocations can be easily emitted from the nearby
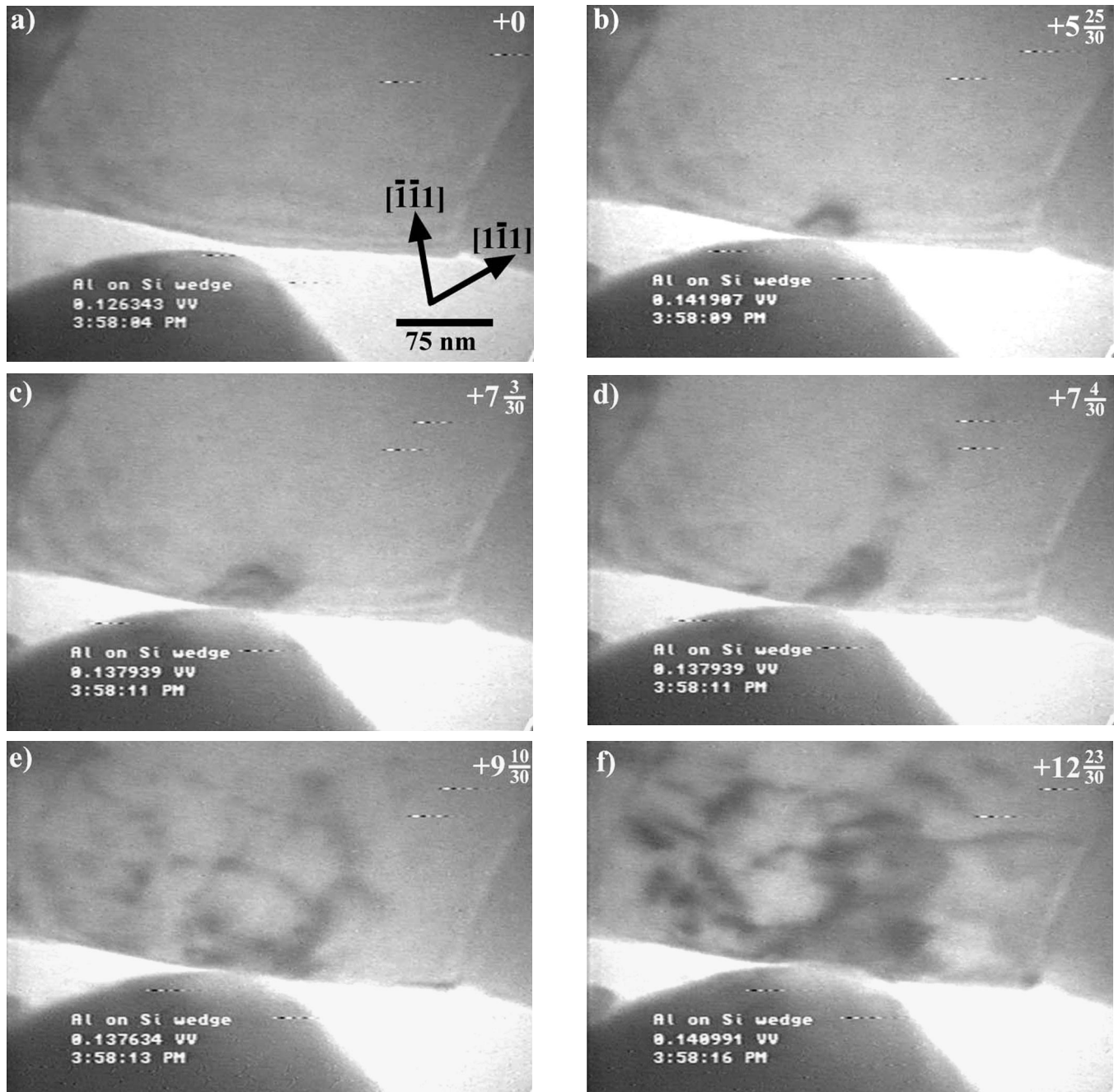
Fig. 6. (a)–(f) The time-series TEM images of an Al grain showing the evolution of elastic-plastic deformation during an in-situ nanoindentation experiment. The direction of indentation is close to [1-11] in the indented grain. The time elapsed from image (a) is given in seconds in the upper right corner of each frame.

grain boundaries in fine-grained samples but must be found or formed in the interiors of grains in coarse-grained samples.

Figure 8 shows a similar result achieved in this study through in-situ nanoindentation tests into Al grains of two different sizes. In-situ nanoindentation has the advantage that the grain size is readily observable and can be determined uniquely for each indentation. In this case, two indentations were made into grains of different diameters. The "large" grain had a grain diameter of 670 nm, which is significantly larger than the indenter radius. The "small" grain had a grain diameter of approximately 100 nm, which is about the same size as the indenter radius. Both grains were approximately 250 nm in thickness. The qualitative indentation responses for the two grains showed the same characteristic difference observed by Lilleodden and Nix for indentations into Au films. The large-grain Hertzian elastic contact was followed by discrete plasticity, while the small grain showed elastic-plastic response from the onset of contact. Included in Fig. 8a is the raw voltage versus displacement responses associated with the indentations into Al. Irrespective of our cal-
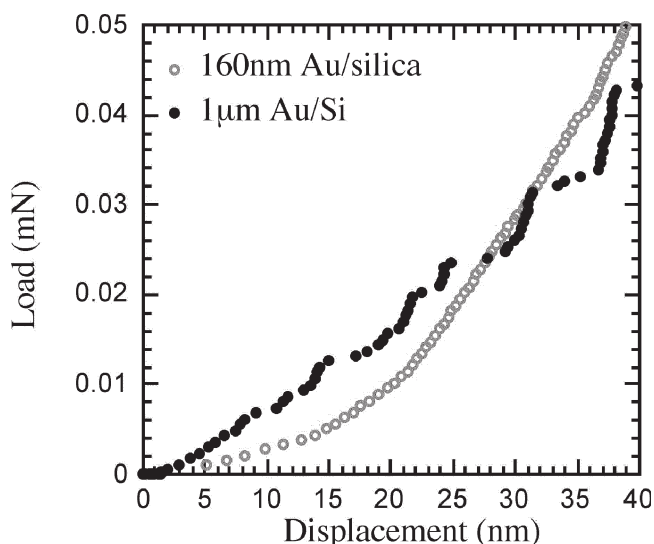
Fig. 7. The results from instrumented indentation experiments into Au thin films of two different nominal-grain sizes conducted by Lilleodden and Nix.[11,12]

ibration, the characteristic difference in indentation response between the large and small grain is still observed.

CONCLUSIONS

It has been shown that in-situ nanoindentation in a TEM is a useful technique to examine the mechanical properties of small volumes. Correlation between quantified load-displacement measurements and the underlying mechanisms associated with small-volume deformation is uniquely achieved using this technique. The methodology used to calibrate the instrument for such quantitative measurements has been detailed. Using this in-situ indentation technique, indentations into Al thin films were conducted. A sharp change in the force-displacement response at the elastic-to-plastic transition has been shown to signify the nucleation of dislocations, as has been implied by indentation investigations. The measured loading behavior was shown to be consistent with high-resolution force-displacement data
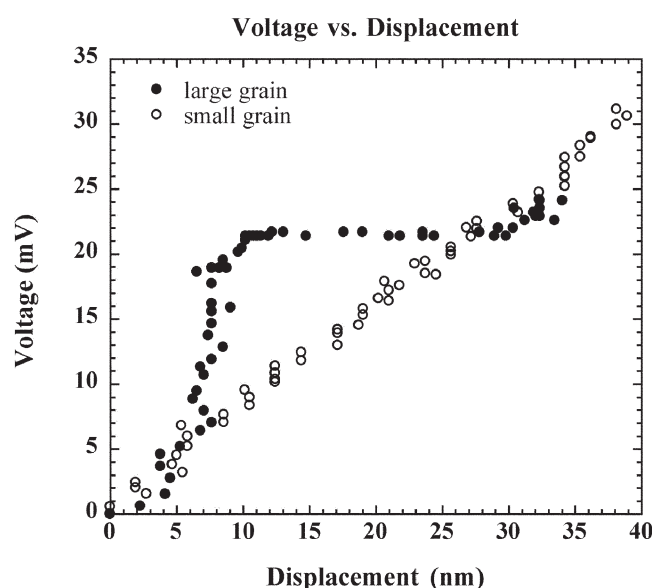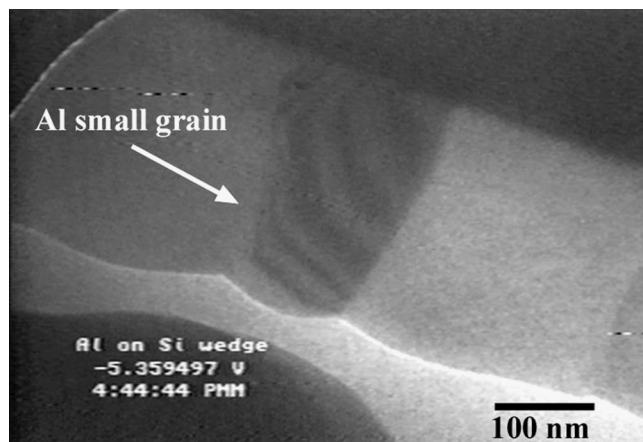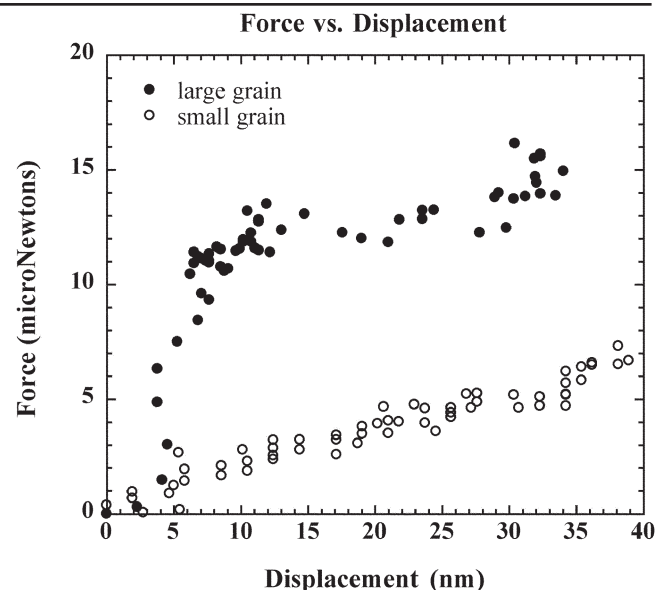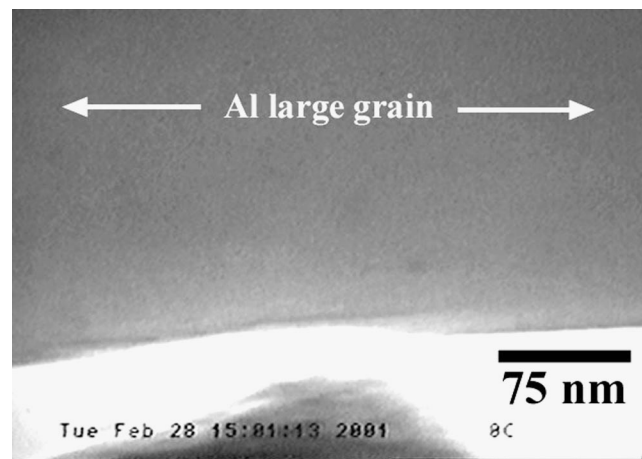

Fig. 8. (a) The voltage-displacement response associated with indentations into two grains of Al with different sizes relative to the indenter. (b) The corresponding calibrated load-displacement response for the same two grains. (c) and (d) The TEM images of the small grain and large grain, respectively, with the diamond indenter approaching the grains before indentation. The grain termed "small grain" had an effective grain size of ~100 nm, about the same size as the indenter radius. The grain termed "large grain" had an effective grain size of ~670 nm, which is large relative to the size of the indenter.

obtained with instrumented indentation techniques. Furthermore, contrasting behaviors in fine- and coarse-grained samples observed in other studies show the same trend observed for indentations into large and small grains in Al.

ACKNOWLEDGEMENTS

REFERENCES

1. J.B. Pethica, R. Hutchings, and W.C. Oliver, *Phil. Mag. A* 48, 593 (1983).
2. W.C. Oliver and G.M. Pharr, *J. Mater. Res.* 7, 1564 (1992).
3. A. Gouldstone, H.-J. Koh, K.-Y. Zeng, A.E. Giannakopoulos, and S. Suresh, *Acta Mater.* 48, 2277 (2000).
4. W.W. Gerberich, J.C. Nelson, E.T. Lilleodden, P. Anderson, and J.T. Wyrobek, *Acta Mater.* 44, 3585 (1996).
5. V. Domnich, Y. Gogotsi, and S. Dub, *Appl. Phys. Lett.* 76, 2214 (2000).
6. For example, *Nanoindenter XP,* MTS Corp., Minneapolis, MN.
7. J.B. Pethica and W.C. Oliver, *Thin Films: Stresses and Mechanical Properties, Proceedings of the Materials Research Society,* ed. J.C. Bravman, W.D. Nix, D.M. Barnett, D.M. and D.A. Smith, (Pittsburgh, PA: Materials Research Soc., 1989), pp. 13–23.
8. K.L. Johnson, *Contact Mechanics* (Cambridge, United Kingdom: Cambridge University Press, 1985).
9. M. Wall and U. Dahmen, *Microsc. Microanalysis* 3, 593 (1997).
10. A.M. Minor, J.W. Morris, and E.A. Stach, *Appl. Phys. Lett.* 79, 1625 (2001).
11. E.T. Lilleodden (Ph.D. thesis, Stanford University, 2001).
12. E.T. Lilleodden and W.D. Nix, submitted to *Acta. Mat.* (2002).
13. S.G. Cocoran, R.J. Colton, E.T. Lilleodden, and W.W. Gerberich, *Phys. Rev. B* 55, R16057 (1997).